Theoretical Study of Atomic Layer Deposition Reaction Mechanism and Kinetics for Aluminum Oxide Formation at Graphene Nanoribbon Open Edges

Kun Xu* and Peide D. Ye

School of Electrical and Computer Engineering and Birck Nanotechnology Center, Purdue University, West Lafayette, Indiana 47907

Received: February 14, 2010; Revised Manuscript Received: April 20, 2010

The atomic layer deposition (ALD) reaction of Al_2O_3 at graphene nanoribbon open edges has been studied theoretically by ab initio density functional theory and transition state rate theory. The structures of reactants, adsorption complexes, products, and transition states of the model reactions were optimized at the B3LYP/6-311G(d,p) level of theory. The potential energy profiles have revealed the mechanisms of the chemical adsorption and the dissociation reactions. The potential barriers of the adsorption reactions for the zigzag edge (eq 1z) and armchair edge (eq 1a) are predicted to be 1.5 and 6.5 kcal/mol, respectively, while in the following steps the adsorption process is a barrierless reaction and the dissociation process undertakes the release of CH_4 via a tight transition state. The reaction rates for all five solid−gas interface reaction steps have been calculated in the temperature range 300−1000 K and the pressure range 0.1 Torr−10 atm. The result shows that the adsorption rate of the zigzag edge with H_2O is much faster than that of the armchair edge with H_2O. Theoretical prediction for reaction temperature and pressure is in good agreement with the experimental conditions. This work outlines a way by ALD to selectively decorate and passivate the zigzag and armchair edges of graphene nanoribbons, which have significantly different electrical and magnetic properties.

1. Introduction

Graphene is a single sheet of hexagonal lattice of carbon atoms, which is formed by a σ_{C-C} bond with a nonlocalized π_{C-C} orbital perpendicular to the graphene plane. The superior electron transport properties of graphene recently have been studied intensively in the condensed matter physics field.[1−3] The electron velocity in graphene is about 10^8 cm·s^{-1} and the mobility of >15 000 cm^2 V^{-1} s^{-1} has been observed at room temperature, which is much higher than those of most semiconductor materials. A brand new class of carbon-based transistors and integrated circuits with performance superior to the current silicon-based technology are expected to be developed. With the recent advance in mass growth of graphene on SiC[4−6] or chemical vapor deposition on Ni[7−9] and Cu[10] emerges, the realization of graphene-based devices seems more and more imminent than ever.

The advantage of epitaxial graphene for nanoelectronic applications resides in its planar two-dimensional structure that enables conventional top-down lithography and processing techniques. Graphene is a semimetal with zero bandgap. Quantum confinement can be used to open a bandgap of several tenths of an electronvolt by forming graphene nanoribbons at 10 nm scale.[11] The nanoribbon edges become extremely important for carrier transport in graphene due to the reduced dimension.[12] Interestingly, only two types of graphene edges, zigzag or armchair, can be formed. The electrical properties of graphene nanoribbons are strongly dependent on the type of edge and the passivation of the C dangling bonds.[13]

Recently, atomic layer deposited (ALD) high-κ dielectric integration on graphene has attracted wide interest.[14−19] A high-quality ultrathin high-κ dielectric, such as the most studied Al_2O_3, is a must for top-gate graphene devices. Experimentally, Al_2O_3 can only be deposited on graphene edges in a typical growth temperature of 400−600 K by alternating the pulse of trimethylaluminum (TMA) and water vapor, because the perfect graphene surface is chemically inert and does not lend itself to the conventional ALD process.[15,16] Although the surface chemistry of the TMA/H_2O process is qualitatively rather well understood, the reaction mechanisms and kinetics have not been elucidated in detail until now. To our knowledge, there are only a few theoretical papers related to the TMA/H_2O reaction mechanism[20−22] and no chemical kinetics studies of the ALD process on the graphene nanoribbon edges. To selectively generate and passivate the zigzag or armchair edge types is critical to fully utilize graphene nanoribbons as the building block for future carbon nanoelectronics.

In this paper, the mechanism of one ALD cycle for TMA/H_2O at the graphene edge is elucidated completely by ab initio density functional theory and solid−gas interface transition state theory. To obtain more reliable results, a sufficiently large model reaction system has been chosen based on our computing resources. The result shows that ALD Al_2O_3 is much more easily deposited on zigzag edges compared to armchair edges in the typical ALD process conditions. The ALD process can be used to selectively decorate and passivate graphene nanoribbon edges. The theoretical predicted result is compared with the available experimental data.

2. Computational Methods

Quantum chemical density functional theory is employed to investigate the model reaction mechanism for the ALD of Al_2O_3 formation on graphene edges. The geometric parameters of the reactants, products, intermediates, and transition states are optimized at the B3LYP/6-311G(d,p) level of theory.[23−25] The harmonic vibrational frequencies of all species and stationary points are calculated with the corresponding optimization method for kinetics calculation. The transition state structures are determined with only one imaginary vibrational mode and the minimum energy pathways are confirmed by the intrinsic reaction coordinate (IRC).[26,27] All the electronic structure calculations are performed by the Gaussian 03 program.[28]

* To whom correspondence should be addressed. E-mail: xu83@purdue.edu.

10.1021/jp101387g © 2010 American Chemical Society
Published on Web 05/25/2010

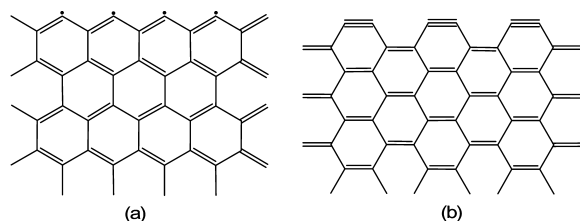

Figure 1. Graphene structures with (a) zigzag edge and (b) armchair edge

3. Results and Discussion

There are two types of graphene nanoribbon open edges, zigzag and armchair, as shown in Figure 1. Each carbon atom of the zigzag edge has an unpaired electron, which is active to combine with other reactants. However, the carbon atoms of the armchair edge side are more stable in chemical reactivity because a triple covalent bond is formed between two open edge carbon atoms of each edge hexagonal ring. To perform accurate quantum chemical calculations, this solid−gas interface reaction is simplified to be a gas phase reaction of didehydronaphthalene ($C_{10}H_6$) with water as well as with trimethylaluminum (TMA). Graphene with a zigzag edge is represented by 1,8-naphthalenediyl (denoted by z-$C_{10}H_6$), while that with an armchair edge by 2,3-naphthalyne (denoted by a-$C_{10}H_6$). The elementary reaction for each deposition step in one deposition cycle can be considered as follows:

$$z\text{-}C_{10}H_6 + H_2O \rightarrow z\text{-}C_{10}H_7OH(P1) \quad (1z)$$

$$a\text{-}C_{10}H_6 + H_2O \rightarrow a\text{-}C_{10}H_7OH \quad (1a)$$

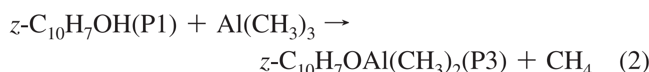

$$z\text{-}C_{10}H_7OH(P1) + Al(CH_3)_3 \rightarrow z\text{-}C_{10}H_7OAl(CH_3)_2(P3) + CH_4 \quad (2)$$

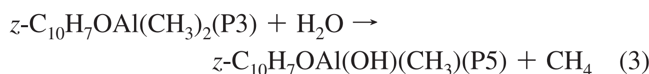

$$z\text{-}C_{10}H_7OAl(CH_3)_2(P3) + H_2O \rightarrow z\text{-}C_{10}H_7OAl(OH)(CH_3)(P5) + CH_4 \quad (3)$$

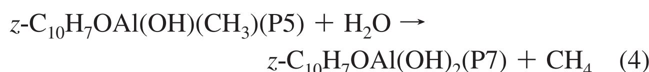

$$z\text{-}C_{10}H_7OAl(OH)(CH_3)(P5) + H_2O \rightarrow z\text{-}C_{10}H_7OAl(OH)_2(P7) + CH_4 \quad (4)$$

$$z\text{-}C_{10}H_7OAl(OH)_2(P7) + Al(CH_3)_3 \rightarrow z\text{-}C_{10}H_7OAl(OH)OAl(CH_3)_2(P9) + CH_4 \quad (5)$$

It is evident that the subsequent reaction steps will repeat the reactions from steps 3 to 5, adding H_2O and then TMA along with the CH_4 gas elimination. To confirm the reliability of this model, we compared the reaction heat of $C_{28}H_{12} + H_2O \rightarrow C_{28}H_{13}OH$ with that of $C_{10}H_6 + H_2O$ at the B3LYP/6-311G(d,p) level of theory. $C_{28}H_{12}$ contains 8 hexagonal rings, as seen in the Supporting Information. The result shows that the heat of reaction values are predicted to be −105.3 and −103.3 kcal/mol for $C_{28}H_{12} + H_2O \rightarrow C_{28}H_{13}OH$ and $C_{10}H_6 + H_2O \rightarrow C_{10}H_7OH$, respectively. The difference is only about 2 kcal/mol (2% error), which is completely within the error range of the calculation methods. In the following reaction steps, the effect of the aromatic graphene system on the reaction is almost negligible because the reaction center is far from it. Thus, it is reasonable to model graphene as didehydronaphthalene for this solid−gas surface reaction mechanism.

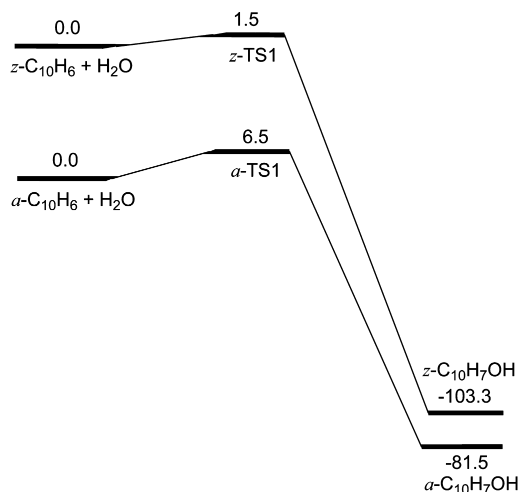

Figure 2. Potential energy profiles of the model reaction of $C_{10}H_6$ with H_2O at the B3LYP/6-311G(d,p) level of theory in units of kcal/mol. z denotes zigzag edge and a denotes armchair edge

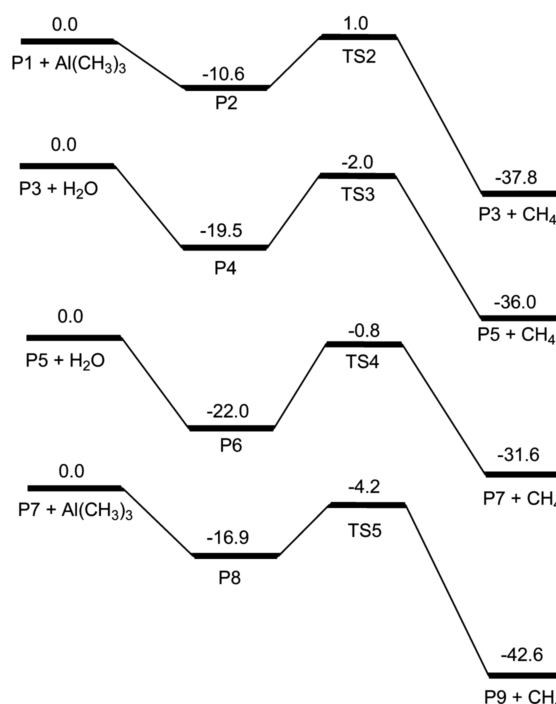

Figure 3. Potential energy profiles of the reactions about the atomic layer deposition of Al_2O_3 on graphene edge at the B3LYP/6-311G(d,p) level of theory in units of kcal/mol.

3.1. ALD Reaction Mechanism. The potential energy profiles of the above five reactions are illustrated in Figures 2 and 3 predicted at the B3LYP/6-311G(d,p) level of theory. The structures of reactants, intermediates, and transition states shown in Figure 4 are optimized at the B3LYP/6-311G(d,p) level of theory. The harmonic vibrational frequencies and the Cartesian coordinates of all species and transition states are summarized in the Supporting Information.

3.1.1. $C_{10}H_6 + H_2O$. This reaction represents the first step of the atomic layer deposition of aluminum oxide on graphene nanoribbon open edges. In the case of 1, 8-naphthalenediyl (z-$C_{10}H_6$) with H_2O, one hydrogen atom of the water molecule approaches the 8-position carbon radical of z-$C_{10}H_6$ via the transition state z-TS1, at which the imaginary frequency is i1305 cm^{-1} and the lengths of the O−H breaking bond and the C−H forming bond are 1.229 and 1.258 Å, respectively. With the

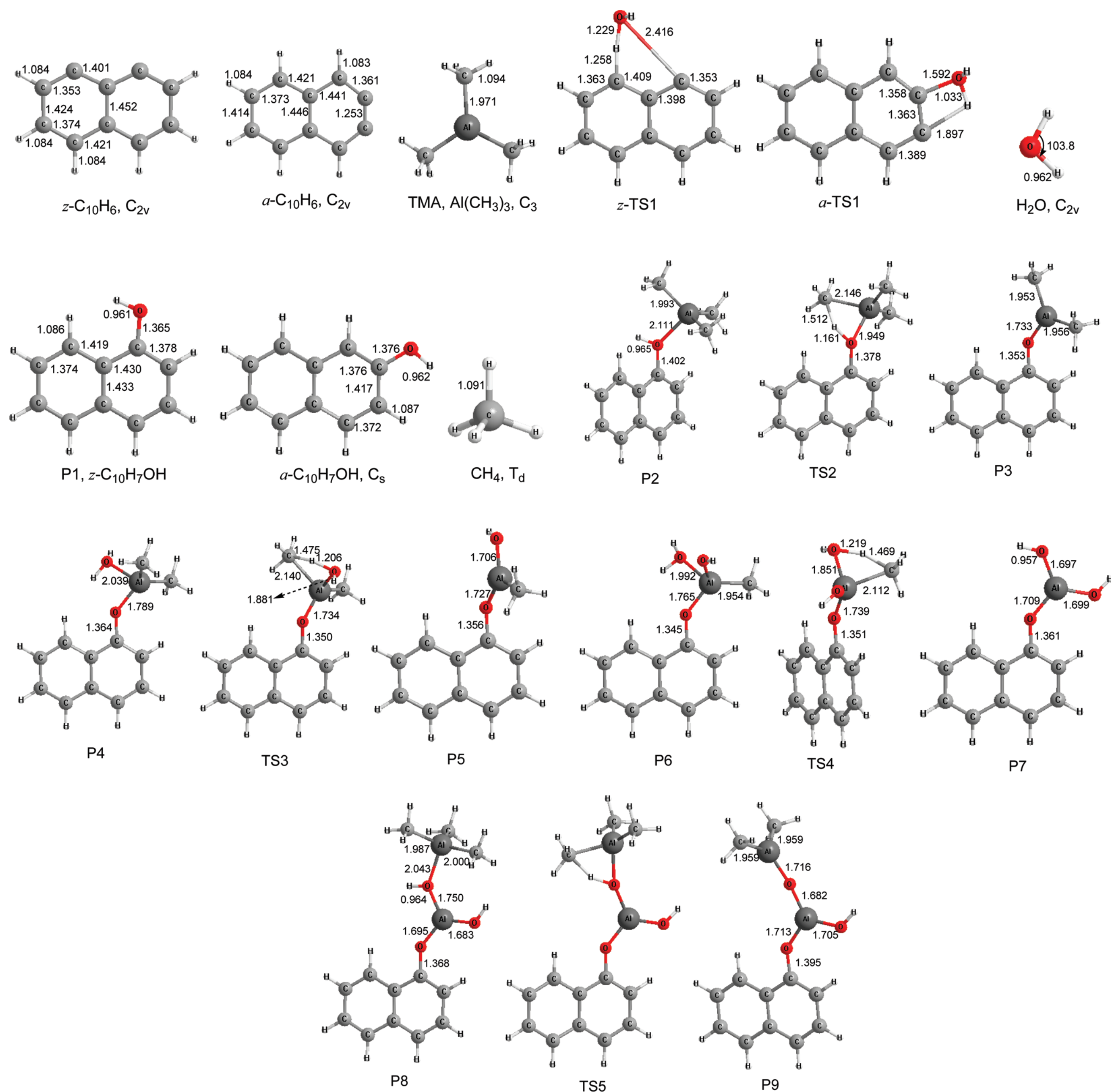

Figure 4. Geometric parameters (bond length in Å and bond angle in deg) of reactants, intermediates, products, and transition states optimized at the B3LYP/6-311G(d,p) level of theory.

H−O bond broken and the C−H bond formed, the OH radical will readily migrate to the 1-position carbon radical to form 1-naphthelenol (z-$C_{10}H_7OH$, P1) with exothermicity of 103.3 kcal/mol. As shown in Figure 2, the forward reaction barrier is predicted to be 1.5 kcal/mol. For the reaction of 2,3-naphthalyne (a-$C_{10}H_6$) with H_2O to produce 2-naphthelenol (a-$C_{10}H_7OH$), it is different from the reaction of z-$C_{10}H_6$ + H_2O. The transition state, *a*-TS1, is predicted to be an approximately four-membered-ring structure with an imaginary frequency of $i232$ cm^{-1}. Thus, the addition reaction between H_2O and the C−C triple bond of a-$C_{10}H_6$ could occur approximately by a concerted process. At *a*-TS1, the O−C and H−C forming bond are 1.592 and 1.897 Å, respectively, while the O−H breaking bond is 1.033 Å. Although the a-$C_{10}H_6$ + H_2O reaction is a strong exothermic process with the exothermicity of 81.5 kcal/mol, its forward reaction barrier of 6.5 kcal/mol is much higher than that of the z-$C_{10}H_6$ + H_2O reaction. This implies the reaction of the zigzag edge graphene with water could take place more readily than that of the armchair edge graphene with water.

3.1.2. P1 + Al(CH₃)₃. Because of the electron-deficient property of trimethylaluminum (TMA), it has a strong tendency to accept an electron pair. The oxygen atom of z-$C_{10}H_7OH$ (P1) can just provide a lone electron pair to donate. Therefore, $Al(CH_3)_3$ is readily combined with P1 to form the intermediate complex, P1-TMA (P2), with the O−Al bond. As shown in Figure 3, the complex, P2, is below the reactants, P1 + $Al(CH_3)_3$, by 10.6 kcal/mol. This association process is a barrierless process as confirmed in Figure 5, in which the minimum energy path is optimized by stretching the O−Al distance of the complex P2 at the B3LYP/6-311G(d,p) level of theory.

The decomposition reaction can further take place from P2 by CH_4 elimination via the transition state TS2. This transition state is a four-membered-ring structure, at which the C−Al and O−H breaking bonds are 2.146 and 1.161 Å, respectively, while

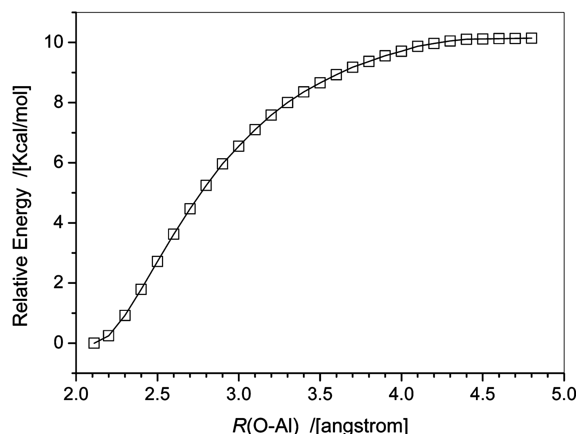

Figure 5. Minimum energy path of the deposition process of P1 with TMA with respect to the O−Al length optimized at the B3LYP/6-311G(d,p) level of theory.

the C−H forming bond is 1.512 Å. The imaginary frequency of TS2 is $i1218$ cm^{-1}. The P3 + CH_4 products lie below the P1 + $Al(CH_3)_3$ reactant by 37.8 kcal/mol and the TS2 is above the reactants by 1.0 kcal/mol.

3.1.3. P3 + H_2O. In this reaction system, the oxygen atom of water, as a strong electron pair donor, can associate with the aluminum atom of P3 first to form the intermediate complex, P4, with an exothermicity of 19.5 kcal/mol, which is 8.9 kcal/mol greater than that of P1 + $Al(CH_3)_3$ → P2. It is apparent that this is a barrierless adsorption process. From P4, the reaction proceeds to eliminate CH_4 via the transition state, TS3, with an imaginary frequency of $i1318$ cm^{-1}. The P5 + CH_4 products and the transition state are below the reactants by 36.0 and 2.0 kcal/mol, respectively. As shown in Figure 4, at this four-membered-ring transition state the C−Al and O−H breaking bonds elongate to 2.140 and 1.206 Å, respectively, while the C−H forming distance shortens to 1.475 Å. Comparing with the P1 + $Al(CH_3)_3$ reaction, the P3 + H_2O reaction could occur with lower relative energy intermediate complex and transition state.

3.1.4. P5 + H_2O. Similar to the P3 + H_2O reaction, the second water molecule is attached to the aluminum atom of P5 by a barrierless association process. The heat released is 22.0 kcal/mol for the formation of the intermediate complex P6, slightly more than the heat released in P3 + H_2O → P4. The transition state, TS4, representing the elimination process of methane from P6 to P7 + CH_4 is a four-membered-ring transition structure with an imaginary frequency of $i1341$ cm^{-1}. At TS4, the C−Al and O−H breaking bonds extend to 2.112 and 1.219 Å, respectively, while the C−H forming distance shortens to 1.469 Å. Because the energies of TS4 and the products, P7 + CH_4, are −0.8 and −31.6 kcal/mol, respectively, relative to the energy of P5 + H_2O, this reaction may happen more readily, too.

3.1.5. P7 + $Al(CH_3)_3$. This reaction is like the reaction of P1 + $Al(CH_3)_3$. First, the reactants associate barrierlessly to the intermediate complex, P8, and then eliminate CH_4 to produce P9 via a transition state, TS5. Figure 3 shows that P8 and TS5 are predicted to be −16.9 and −4.2 kcal/mol relative to the reactants P7 + $Al(CH_3)_3$. Comparing with the P1 + $Al(CH_3)_3$ reaction, the P7 + $Al(CH_3)_3$ reaction should take place more rapidly. This difference may be due to the different atomic charges of the oxygen atoms in P1 and P7. At the B3LYP/6-311G(d,p) level, the Mulliken atomic charge of the O atom of P1 is −0.3535e; however, that of the O atom of P7 is −0.6422e, which is twice as much as the previous charge. The electron-deficient TMA can combine more readily with P7 to form the O−Al bond with more exothermicity. From Figure 3, one can observe that the releasing energy of P1 + TMA → P2 is 10.6 kcal/mol, which is 6.3 kcal/mol less than that of P7 + TMA → P8. Because the reaction barrier height (11.6 kcal/mol) of P2 → P3 + CH_4 is similar to that (12.7 kcal/mol) of P8 → P9 + CH_4, it results in a TS2 higher than that of P1 + TMA, and a TS5 lower than that of P7 + TMA in energy.

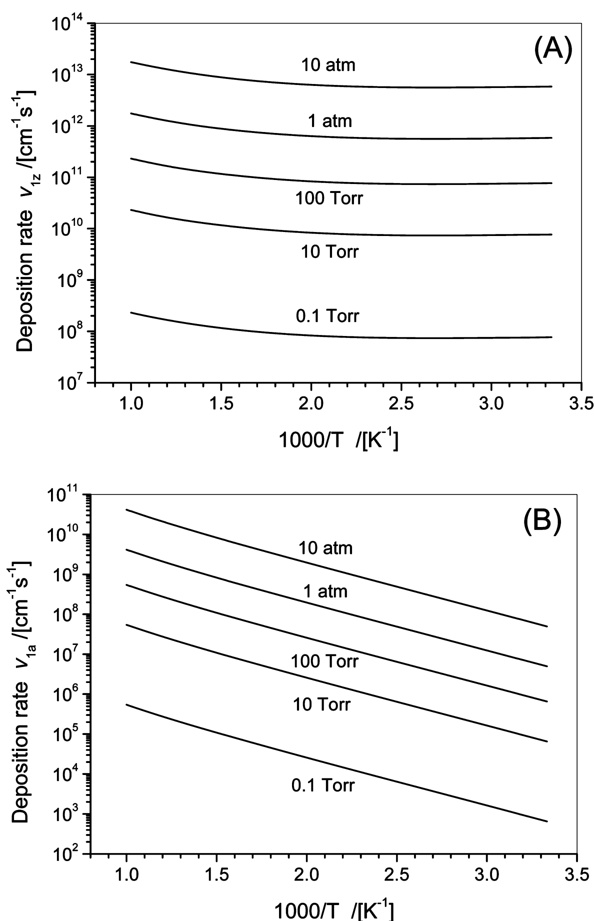

Figure 6. Predicted chemical adsorption rates of reactions 1z (A) and 1a (B).

3.2. ALD Solid−Gas Interface Reaction Rates. The above solid−gas interface reaction mechanisms may be represented by the reaction scheme:

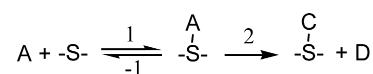

A and D are gas molecules, while −S−, −S(A)−, and −(C)S− are solid surface molecular formulas. The interface reaction kinetic equations can be expressed as:

$$\frac{d[AS]}{dt} = k_1[A][S] - k_{-1}[AS] - k_2[AS] \tag{6}$$

$$\frac{d[CS]}{dt} = k_2[AS] \tag{7}$$

where k_1 is the adsorption reaction rate constant and k_{-1} and k_2 are the desorption reaction rate constants. Under the steady state approximation, d[AS]/dt = 0 when [AS] keeps the invariance. Then,

$$\frac{d[CS]}{dt} = \frac{k_2 k_1}{k_{-1} + k_2}[A][S] \quad (8)$$

Because k_2 is much less than k_{-1} in this study, eq 8 can be rewritten approximately as

$$\frac{d[CS]}{dt} = Kk_2[A][S] \quad (9)$$

where $K = k_1/k_{-1}$ is the equilibrium constant for A + S = AS. It can be calculated by $\ln K = -\Delta G/RT$. ΔG here is the change of free energy from A + S to AS, T is the temperature, and R is the gas constant.

According to the absolute rate theory of the solid−gas interface reaction, Laidler[29] suggested the adsorption reaction rate formula

$$v_a = c_g \frac{1}{2} sL \frac{f^{\neq}}{F_g f_s} \exp\left(-\frac{E_0}{RT}\right) \quad (10)$$

and the desorption reaction rate formula

$$v_d = \frac{1}{2} sL \frac{f^{\neq}}{f_s} \exp\left(-\frac{E_0}{RT}\right) \quad (11)$$

Because the reaction interface of graphene in this study is the graphene nanoribbon open edge, the adsorption sites are the carbon atoms on the edge and the reaction interface is a linear lattice. Therefore, in eqs 10 and 11, s is the coordinate number and equals 2; L is the number of single adsorption sites per length unit; c_g is the concentration of gas molecule; E_0 is the potential barrier of the adsorption or desorption reaction; F_g is the partition function of gas phase reactant molecule; and $f^{\neq}$ and f_s are the partition functions of the transition states and solid state reactant, respectively. However, neither of two contains 3-dimension translational motion and 3-dimension rotational motion.

On the basis of the above reaction mechanisms as in Figures 2 and 3 and the harmonic frequencies and structures of the reactants, products, intermediate complexes, and transition states as in the Supporting Information, the ALD reaction rates have been calculated with eqs 9, 10, and 11 in the temperature range from 300 to 1000 K at the gas reactant pressures of 0.1 Torr, 10 Torr, 100 Torr, 1 atm, and 10 atm. The calculation results of the chemical adsorption of H_2O on the graphene edge are shown in Figure 6. It can be seen that the adsorption rates of the zigzag edge, v_{1z}, show smaller positive temperature dependence, while those of the armchair edge, v_{1a}, exhibit stronger positive temperature dependence, because of their intrinsic positive potential barriers. Both v_{1z} and v_{1a} increase with the increasing pressure of H_2O vapor. However, v_{1z} is much more than v_{1a}, because the forward reaction barrier of reaction 1z is much less than that of reaction 1a. From Figure 6, one can see that, at H_2O vapor pressure of 0.1 Torr, v_{1z} is more than about 10^8 cm^{-1} s^{-1} in 300−1000 K, which implies the zigzag edge can be completely saturated by H_2O molecules at the low pressure of H_2O vapor in 1 s duration because $L = 4.02 \times 10^8$

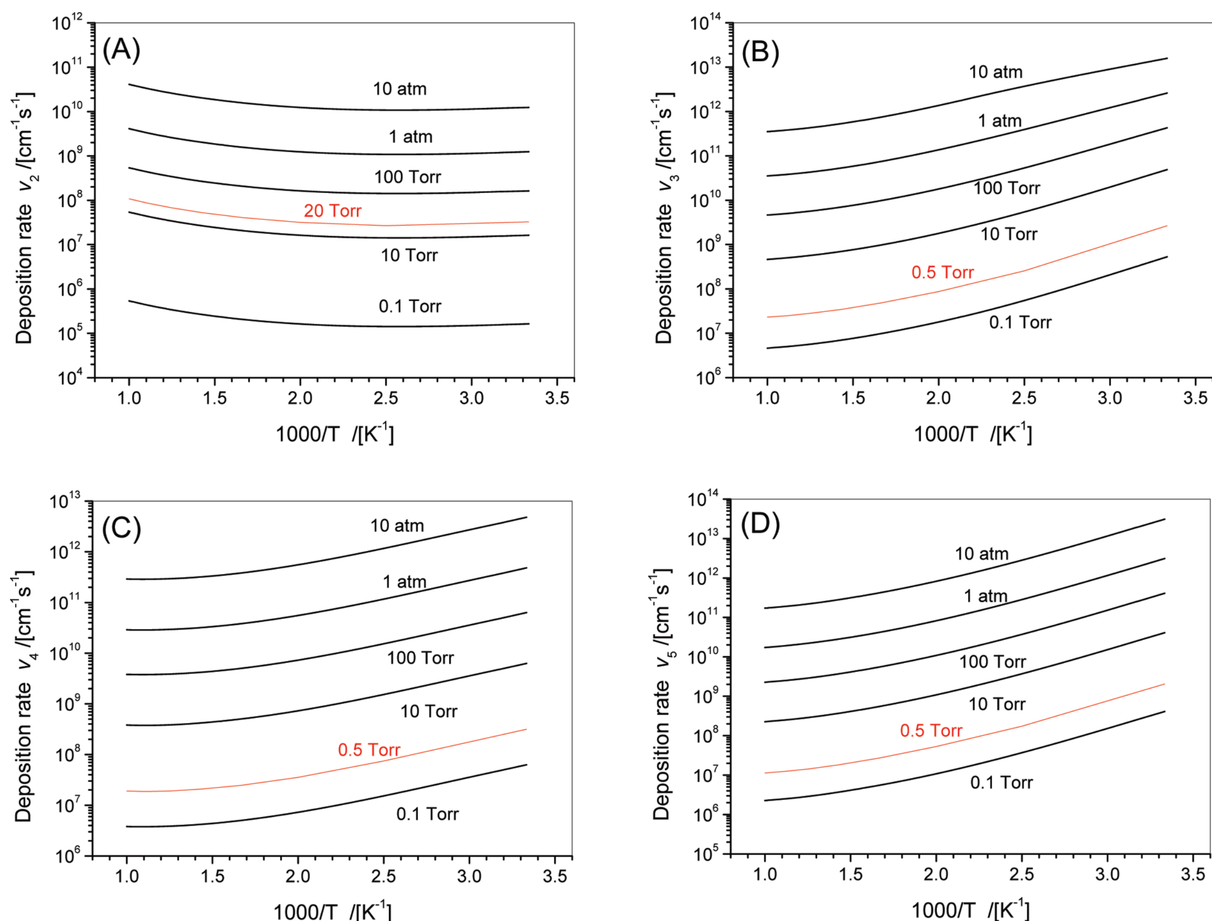

Figure 7. Predicted atomic layer deposition rates of reactions 2 (A), 3 (B), 4 (C), and 5 (D).

adsorption sites per centimeter of the zigzag edge; but the full coverage of the armchair edge in 1 s requires the vapor pressure of H_2O to be at least 100 Torr and a temperature of 500 K.

The predicted rates of the next ALD reaction steps are shown in Figure 7. Each of these reactions is a continuous adsorption and desorption process. The adsorption compound as a reaction intermediate complex can dissociate to release either the initial gas reactant or methane molecule. Because there is no tight transition state in the adsorption process, the desorption reaction back to the reactants is more competitive than the continuous dissociation process. From Figure 7, it can be seen that the rate of reaction 2 has a slightly positive temperature dependence becasue its transition state, TS2, is 1.0 kcal/mol over the reactants. However, the rates of reactions 3, 4, and 5 are remarkably negatively temperature dependent. This means that the Al_2O_3 film growth rate per cycle decreases with temperature increasing, which agrees well with the experimental observations.[17,18] The rates of all four reactions increase along with the increasing pressure of the gas reactants, as in the case of reaction 1. Nevertheless, the rates of reaction 2 are much less than those of the other three reactions. Figure 7A suggests the TMA pressure of over 20 Torr to complete releasing CH_4 thoroughly in 1 s duration from P2. However, in order to complete reactions 3 and 4 in 1 s duration, the minimum pressure of 0.5 Torr for the H_2O vapor is necessary, as shown in Figure 7, panels B and C. For reaction 5, adding TMA and releasing CH_4, its rate is greater than that of reaction 2 because the tight transiton state of reaction 5 is lower than that of the reactants by 4.2 kcal/mol. Figure 7D shows that this reaction requires the TMA gas pressure over 0.5 Torr and the temperature below 700 K to complete this reaction thoroughly in 1 s. Experimentally, ALD Al_2O_3 is deposited on the graphene edge at a growth temperature of 400−600 K and in around 1 s duration.[14−18] It is apparent that the theoretical prediction is in accordance with the experimental conditions and is suggestive of improving experimental condition. For application, the theoretical predicted reaction rates are fitted into the three-parameter formulas:

$$v_{1z} = p_g(1.65 \times 10^{-1})T^{3.21} \exp(1181/T)$$

$$v_{1a} = p_g(6.59 \times 10^{4})T^{0.978} \exp(-2363/T)$$

$$v_{2} = p_g(1.17 \times 10^{-6})T^{4.00} \exp(1532/T)$$

$$v_{3} = p_g(1.04 \times 10^{-6})T^{3.97} \exp(4047/T)$$

$$v_{4} = p_g(4.58 \times 10^{-4})T^{3.23} \exp(2868/T)$$

$$v_{5} = p_g(8.59 \times 10^{-7})T^{3.87} \exp(4200/T)$$

in units of cm^{-1} s^{-1} in the temperature range from 300 to 1000 K, where p_g is the adsorbed gas pressure in units of Torr.

4. Conclusions

The potential energy profiles at the B3LYP/6-311G(d,p) level of theory indicate that the potential barriers of the adsorption reactions 1z and 1a are predicted to be 1.5 and 6.5 kcal/mol, respectively. In subsequent ALD steps, the adsorption processes of TMA and water are all barrierless association reactions. The dissociation reactions proceed via the tight transition states, releasing CH_4, which are predicted to be lower than the reactants in energy, with the exception of TS2. Each of the ALD steps is a strong exothermic process.

The adsorption rate of the zigzag edge with H_2O is much faster than that of the armchair edge with H_2O. The zigzag edge can be completely saturated by H_2O molecules in 1 s at 0.1 Torr and >300 K, while the full coverage of the armchair edge in 1 s would require the vapor pressure of H_2O to be at least 100 Torr and a temperature of 500 K. v_{1z} and v_{1a} are positively temperature dependent. However, the rates of succeeding ALD cycle reactions are negatively temperature dependent. This theoretical prediction is in good agreement with the available experimental observations. With the exception that the process of P1 + $Al(CH_3)_3 \rightarrow$ P3 + CH_4 is predicted to complete in 1 s at least 20 Torr pressure, all other processes could complete in 1 s at 0.5 Torr.

Acknowledgment. The authors would like to thank Prof. M. C. Lin, Dr. Z. F. Xu and Dr. Y. Xuan for the technical assistance and valuable discussions. Part of the work on graphene is supported by NRI (Nanoelectronics Research Initiative) through MIND (Midwest Institute of Nanoelectronics Discovery), DARPA, and Intel Cooperation.

Supporting Information Available: Table of geometric parameters and frequencies of all species optimized at the B3LYP/6-311G** level of theory. This material is available free of charge via the Internet at http://pubs.acs.org.

References and Notes

(1) Geim, A. K.; Novoselov, K. S. *Nat. Mater.* **2007**, *6*, 183.
(2) Novoselov, K. S.; Geim, A. K.; Morozov, S. V.; Jiang, D.; Zhang, Y.; Dubonos, S. V.; Grigorieva, I. V.; Firsov, A. A. *Science* **2004**, *306*, 666.
(3) Zhang, Y.; Tan, Y. W.; Stormer, H. L.; Kim, P. *Nature* **2005**, *438*, 201.
(4) Berger, C.; Song, Z.; Li, X.; Wu, X.; Brown, N.; Naud, C.; Mayou, D.; Li, T.; Hass, J.; Marchenkov, A. N.; Conrad, E. H.; First, P. N.; de Heer, W. A. *Science* **2006**, *312*, 1191.
(5) Wu, Y. Q.; Ye, P. D.; Capano, M. A.; Xuan, Y.; Sui, Y.; Qi, M.; Cooper, J. A.; Shen, T.; Pandey, D.; Prakash, G.; Reifenberger, R. *Appl. Phys. Lett.* **2008**, *92*, 092102.
(6) Shen, T.; Gu, J. J.; Xu, M.; Wu, Y. Q.; Bolen, M. L.; Capano, M. A.; Engel, L. W.; Ye, P. D. *Appl. Phys. Lett.* **2009**, *95*, 172105.
(7) Kim, K. S.; Zhao, Y.; Jang, H.; Lee, S. Y.; Kim, J. M.; Kim, K. S.; Ahn, J.-H.; Kim, P.; Choi, J.-Y.; Hee Hong, B. H. *Nature* **2009**, *457*, 706.
(8) Reina, A.; Jia, X.; Ho, J.; Nezich, D.; Son, H.; Bulovic, V.; Dresselhaus, M. S.; Kong, J. *Nano Lett.* **2009**, *9*, 30.
(9) Yu, Q.; Lian, J.; Siriponglert, S.; Li, H.; Chen, Y. P.; Pei, S.-S. *Appl. Phys. Lett.* **2008**, *93*, 113103.
(10) Li, X.; Cai, X.; An, J.; Kim, S.; Nah, J.; Yang, D.; Piner, R.; Velamakanni, A.; Jung, I.; Tutuc, E.; Banerjee, S. K.; Colombo, L.; Ruoff, R. S. *Science* **2009**, *324*, 1312.
(11) Han, M. Y.; Brant, J. C.; Kim, P. *Phys. Rev. Lett.* **2010**, *104*, 056801.
(12) Wang, X. R.; Ouyang, Y. J.; Li, X. L.; Wang, H. L.; Guo, J.; Dai, H. J. *Phys. Rev. Lett.* **2008**, *100*, 206803.
(13) Liang, G. C.; Neophytou, N.; Nikonov, D. E.; Lundstrom, M. S. *IEEE Trans. Electron Devices* **2007**, *54*, 677.
(14) Puurunen, R. L. *J. Appl. Phys.* **2005**, *97*, 121301.
(15) Xuan, Y.; Wu, Y.; Shen, Q.; Qi, T. M.; Capano, M. A.; Cooper, J. A.; Ye, P. D. *Appl. Phys. Lett.* **2008**, *92*, 013101.
(16) Wang, X.; Tabakman, S. M.; Dai, H. *J. Am. Chem. Soc.* **2008**, *130*, 8152.
(17) Aarik, J.; Aidla, A.; Jaek, A.; Kiisler, A. A.; Tammik, A. A. *Acta Polytech. Scand., Chem. Technol. Metall. Ser.* **1990**, *195*, 201.
(18) Elliott, S. D.; Scarel, G.; Wiemer, C.; Fanciulli, M.; Pavia, G. *Chem. Mater.* **2006**, *18*, 3764.
(19) Williams, J. R.; DiCarlo, L.; Marcus, C. M. *Science* **2007**, *317*, 638.
(20) Widjaja, Y.; Musgrave, C. B. *Appl. Phys. Lett.* **2002**, *80*, 3304.
(21) Heyman, A.; Musgrave, C. B. *J. Phys. Chem. B* **2004**, *108*, 5718.
(22) Elliott, S. D.; Greer, J. C. *J. Mater. Chem.* **2004**, *14*, 3246.
(23) Lee, C.; Yang, W.; Parr, R. G. *Phys. Rev. B* **1988**, *37*, 785.
(24) Miehlich, B.; Savin, A.; Stoll, H.; Preuss, H. *Chem. Phys. Lett.* **1989**, *157*, 200.
(25) Becke, A. D. *J. Chem. Phys.* **1993**, *98*, 5648.

(26) Fukui, K. *Acc. Chem. Res.* **1981**, *14*, 363.

(27) Hratchian, H. P.; Schlegel, H. B. In *Theory and Applications of Computational Chemistry: The First 40 Years*; Dykstra, C. E., Frenking, G., Kim, K. S., and Scuseria, G., Eds.; Elsevier: Amsterdam, The Netherlands, 2005, 195−249.

(28) Frisch, M. J.; Trucks, G. W.; Schlegel, H. B.; Scuseria, G. E.; Robb, M. A.; Cheeseman, J. R.; Montgomery, J. A., Jr.; Vreven, T.; Kudin, K. N.; Burant, J. C.; Millam, J. M.; Iyengar, S. S.; Tomasi, J.; Barone, V.; Mennucci, B.; Cossi, M.; Scalmani, G.; Rega, N.; Petersson, G. A.; Nakatsuji, H.; Hada, M.; Ehara, M.; Toyota, K.; Fukuda, R.; Hasegawa, J.; Ishida, M.; Nakajima, T.; Honda, Y.; Kitao, O.; Nakai, H.; Klene, M.; Li, X.; Knox, J. E.; Hratchian, H. P.; Cross, J. B.; Bakken, V.; Adamo, C.; Jaramillo, J.; Gomperts, R.; Stratmann, R. E.; Yazyev, O.; Austin, A. J.; Cammi, R.; Pomelli, C.; Ochterski, J. W.; Ayala, P. Y.; Morokuma, K.; Voth, G. A.; Salvador, P.; Dannenberg, J. J.; Zakrzewski, V. G.; Dapprich, S.; Daniels, A. D.; Strain, M. C.; Farkas, O.; Malick, D. K.; Rabuck, A. D.; Raghavachari, K.; Foresman, J. B.; Ortiz, J. V.; Cui, Q.; Baboul, A. G.; Clifford, S.; Cioslowski, J.; Stefanov, B. B.; Liu, G.; Liashenko, A.; Piskorz, P.; Komaromi, I.; Martin, R. L.; Fox, D. J.; Keith, T.; Al-Laham, M. A.; Peng, C. Y.; Nanayakkara, A.; Challacombe, M.; Gill, P. M. W.; Johnson, B.; Chen, W.; Wong, M. W.; Gonzalez, C.; Pople, J. A. *Gaussian 03*, revision C.02; Gaussian, Inc., Wallingford, CT, 2004.

(29) Laidler, K. J. *Chemical Kinetics*, 2nd ed.; McGraw-Hill Book Company, New York, 1965; Chapter 6.

JP101387G